HiSST: 3rd International Conference on
High-Speed Vehicle Science & Technology
14–19 April 2024, Busan, Korea

Computational Parametric Study Evaluating Ramjet Combustor Geometry

David J. Cerantola[1] *Dan Handford*[2] *Pradeep Dass*[3]

Abstract

Leveraging computational fluid dynamics to design ramjet combustors requires a trade-off between solution fidelity and imposed assumptions. Many previous analyses decoupled the combustor from the adjacent components to increase confidence in the complex chemistry were at the expense of neither capturing flow distortion impact on thrust nor nozzle surface temperatures in excess of material limitations. Given the expectation that a lower fidelity approach can capture bulk flow trends from gaseous-hydrogen and air combustion, the 2D computational domain considered in this paper evaluated both the combustor and converging-diverging nozzle sections with the realizable k-ε turbulence model, two-step reaction mechanism, and turbulence chemistry interactions equated using the eddy dissipation concept.
A baseline study that varied flight Mach number (M_0) between 3 and 5 and dynamic pressure between 21 kPa and 76 kPa (3–11 psi) showed that specific impulse (I_{sp}) varied between 2400 s and 3600 s as a function of M_0 with maximum wall and liner temperatures staying below suggested limits 1300 K and 1770 K respectively. A geometric study that varied injector, flameholder, and liner parameters at $M_0 = 3$ or 5 and 5 psi operating conditions found that performance was most strongly influenced by equivalence ratio φ and liner length L_{26} where maximizing L_{26} was beneficial for thrust but $L_{26} < 1$ m was required to respect the temperature limits. Setting $\varphi = 0.7$ resulted in maximum $I_{sp} > 3800$ s whereas thrust was maximum when $\varphi = 1.1$. The best configuration had no appreciable change in I_{sp} but increased thrust by 41% and 7% at the M_0 =3 and 5 conditions respectively relative to the baseline results. Conclusions identify how the geometric parameters response variability can be leveraged to improve design.

Keywords: *Ramjet, Combustor, Nozzle, Hydrogen, CFD*

Nomenclature

Latin

A – pre-exponential factor
alt – altitude, m
BPR – bypass ratio
BR – flameholder blockage ratio
C_D – drag coefficient
E – activation energy
H – height, m
I_{sp} – specific impulse, s
k – turbulence kinetic energy, m2/s2
kb, kf – backward,forward reaction rate
FAR – fuel-air-ratio
L – length, m
L_f – flame length, m
M – Mach number
N – Arrhenius temperature exponent
P – total pressure, Pa
p_{dyn} – freestream dynamic pressure, psi
ps – static pressure, Pa
Re – Reynolds number per unit length, 1/m
T – total temperature, K
$\mathcal{T}$ – net thrust, N
ts – static temperature, K
W – mass-flow rate per unit width, kg/m-s
U – axial velocity, m/s
$\mathcal{V}_{liner}$ – liner volume per unit width, m3/m
(x, y) – Cartesian coordinates with origin at centre flameholder, m

Greek

ΔX_{H2} – horizontal distance between injector and

[1] *Space Engine Systems, Edmonton, Canada, T6R 3L6, dcerantola@spaceenginesystems.com*
[2] *Space Engine Systems, Edmonton, Canada, T6R 3L6*
[3] *Space Engine Systems, Edmonton, Canada, T6R 3L6*

flameholder, m
ΔY_{FH} – vertical distance between flameholders, m
θ_{FH} – flameholder half-angle, deg
θ_{26} – liner angle, deg
ρ – density, kg/m3
ϕ_{26} – liner porosity
φ – equivalence ratio
χ_{FH} – multiple on height between the liner and adjacent flameholder.

Subscripts
0 – freestream
7 – air inlet
7.5 – combustor trailing edge
8 – nozzle throat
9 – nozzle exit
15 – bypass inlet
16 – bypass outlet
26 – cooling liner
H2 – injector inlet

1. Introduction

Ramjet combustor design requires a delicate compromise between achieving thrust requirements and material limitations. At altitude, thrust margins decrease due to higher drag [1] such that propulsion gains from increasing the flame temperature with richer mixtures is desirable for aerodynamics. Unfortunately, preventing deformation and softening caused by increased thermal loads on the materials is at the expense of increased weight, complexity, or cost. Due to the variation in mass flow and temperature throughout the Mach and altitude flight envelope, an opportunity exists to better inform ramjet combustor design by simultaneously evaluating exhaust nozzle wall temperature. In doing so, a more representative accounting of the flight article occurs since the interface between the combustor and nozzle is removed. Although mission profiles are typically not as broad for turbines or scramjets, after-burner and scramjet combustor designs would also benefit from a coupled analysis approach. Additionally, those simulating turbulent non-premixed gaseous hydrogen (H2)-air reactions could gain some insight from this work.

Numerically simulating chemical kinetics remains a difficult challenge. For hydrogen reactions with air, analyses have implemented models including one-step [2], two-step [3], seven step [4], and 38-step elementary [5]. Whereas many publications conducted 2D or simple 3D geometry simulations assuming either inviscid flow [6] or turbulence equated with the Reynolds-Averaged Navier-Stokes (RANS) equations [7–12], more recent efforts have conducted large eddy simulations (LES) [13–15], or direct numerical simulations (DNS) [16, 17]. Despite the capability to evaluate combustion with higher fidelity models, hardware limitations restrict these analyses to relatively smaller computational domains where interfaces are required to decouple the combustion simulation from the upstream and downstream components. Alternatively, lower fidelity approaches have shown reasonable bulk flow agreement and offer the capability to reduce boundary condition definition assumptions at interfaces and conduct parametric studies during the initial design stages to reduce the design space.

Many numerical H2-air reacting flow studies focused on documenting metrics including temperature, velocity, or species profiles, and combustion efficiency in an attempt to articulate mixing and combustion features [7, 8, 11, 13–19]. The motivation for many recent efforts involving H2 fuel was to reduce environmental impact [12, 15, 20]. Unfortunately, this focus is ill-suited for informing gaseous-H2-fueled ramjet combustor design with a bluff-body flameholder. As a result, guidance to set-up a CFD study involving turbulent, non-premixed H2 jets in a co-flow is neither apparent nor are the evaluated operating conditions representative of those experienced by a ramjet in flight.

Fluid dynamics analyses for turbine, ramjet, or rocket nozzles were typically decoupled from combustor simulations since their primary objective was to evaluate thrust. In some cases, there was recognition of surface temperature constraints; however, many of these simulations assumed uniform frozen-flow at the inlet boundary. To appreciate the impact of an uniform flow simulation, Zhang *et al.* [21] observed that distorted flow at a single expansion ramp nozzle throat with exit Mach above 2 reduced thrust by 3–6% and pitch moment by 3–7%. Alternatively, Jia *et al.* [22] observed that a heat shield in an afterburner reduced thermal mixing efficiency by 5.4% caused by a core flow area decrease.

The application of interest is a ramjet combustor consisting of a fuel injector and V-shaped gutter flameholder where the ramjet operates between 3 < Mach < 5. The purpose of this paper is to appreciate

the impact that flight Mach and altitude have on propulsive efficiency and surface temperature and to identify opportunities to maximize thrust with minimum weight. Given that the design space considers both the combustor and nozzle components, the scope is limited to a 2D steady-RANS analysis employing the realizable k-ε turbulence model and two-step H2-air reaction mechanism. Section 2 describes the problem setup and Sec. 3 outlines the CFD methodology. Results to a baseline study that varied M_0 and alt, and a geometric parametric study are in Sec. 4 and conclusions are in Sec. 5.

2. Problem Description

2.1. Geometry

Figure 1 is a schematic showing the combustor–nozzle setup and geometric parameters. The injector, flameholder, and cooling liner features implemented in this study were inspired by afterburner configurations [22–25].Although modifications have been proposed to improve flameholder performance [26], the V-gutter bluff body was chosen given its simplicity to parameterize. Hydrogen is injected horizontally into the flow through five injectors located directly upstream from V-gutter flameholders. The nozzle outlet height $H_9 = 0.84$ m was selected as an ideal expansion value at $M_0 = 3$ and $p_{pdyn} = 5$ psi; therefore, higher M_0 would have under-expanded flow. Ignitor parameters included the injector height H_{H2} and upstream offset from the flameholders ΔX_{H2}. Flameholder parameters included the gutter half-angle θ_{FH}, blockage ratio BR that correlated to height

$$H_{FH} = \frac{H_7 - 2H_{15}}{5} BR \tag{1}$$

spacing between flameholders ΔY_{FH}, and χ_{FH} factor added to the height between the adjacent flameholder and liner. Liner parameters included length L_{26}, angle θ_{26}, porosity ϕ_{26}, and bypass channel height H_{15}.

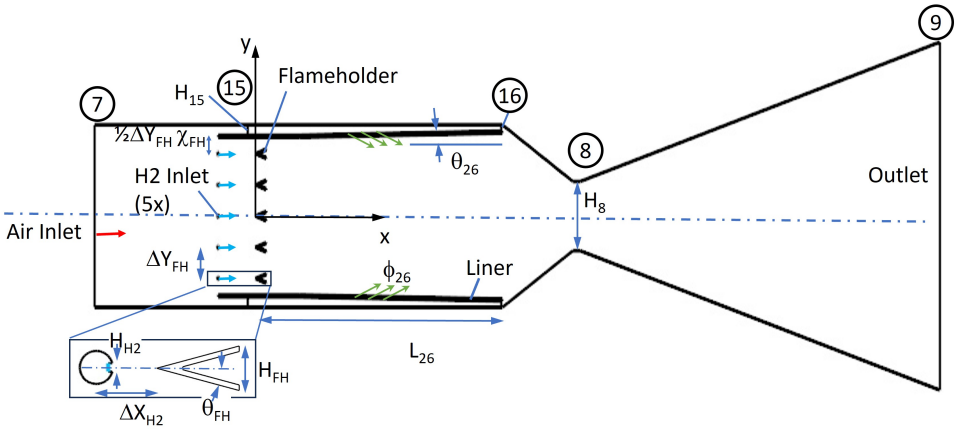

Fig 1. Parameterized geometry schematic.

2.2. Operating Conditions

Following studies completed by Cerantola *et al.* [1, 27], the operating range of interest for the ramjet is between $3 < M_0 < 5$ and $21 < p_{dyn} < 76$ kPa ($3 < p_{dyn} < 11$ psi) dynamic pressure. Air inlet total temperature T_7 was known given M_0 and alt, and flow rate $W_0 = \rho_0 U_0 H_0$ (per unit width) was calculated using the capture area correlation

$$H_0 = \frac{M_0 - 3}{2} (0.5 - 0.32) + 0.32 \tag{2}$$

Nozzle height was obtained from

$$H_8 = \frac{W_0 (1 + FAR)}{\rho_8 U_8} \tag{3}$$

where it was assumed that the throat was sonic with density ρ_8 obtained from $T_8 = 2700$ K and total pressure

$$P_8 = \left(\frac{M_0 - 3}{2} (0.2 - 0.52) + 0.52 \right) P_0 \tag{4}$$

where the high pressure loss is typical for an inlet shocking a supersonic flow down to subsonic. Hydrogen flowrate was parameterized as $W_{H2} = FAR\, W_7$ and total temperature $T_{H2} = 500$ K was assumed.

2.3. Performance Metrics

Propulsive force was evaluated using the net thrust (per unit width) definition

$$\mathcal{T} = W_9 U_9 - W_7 U_0 + H_9 \left(ps_9 - ps_0 \right) \tag{5}$$

And propulsive efficiency was calculated as specific impulse

$$I_{sp} = \frac{\mathcal{T}}{W_{H2}\, g} \tag{6}$$

for g gravity.

Metrics to inform component weight included the liner volume $\forall_{liner}$, maximum liner static temperature $ts_{max,liner}$ and maximum nozzle static temperature $ts_{max,wall}$. To help advise the adequacy of the combustor to contain the flame requires knowledge of the flame length. Unfortunately, there is not a preferred definition or measurement technique for flame length where visual determinations typically are longer than those evaluated from temperature or concentration [28]. For turbulent nonpremixed flames in the momentum-dominated regime, Delichatsios [29] proposed

$$L^* = \frac{L_f\, FAR_s}{d_{H2} \left(\rho_{H2} / \rho_7 \right)^{1/2}} = 23 \tag{7}$$

where L_f is the flame length, $FAR_s = 0.03$ is the stoichiometric mixture fraction for H2-air, $d_{H2} \equiv 2H_{H2}$ is the initial jet diameter and ρ_{H2}/ρ_7 is the H2-to-inlet-air density ratio. In the present study, attempts to evaluate flame length along the centreline where $ts = 0.99 ts_{max}$ or $FAR = 0.003$ yielded many values that suggested the flame extended beyond the nozzle outlet. This was deemed an unlikely result that was suspected to be a consequence of either the simplified reaction mechanism or decreased turbulent mixing associated with k-ε turbulence models.

3. Numerical Methodology

The commercially available CFD code Siemens STAR-CCM+© version 2310 [30] was utilized to obtain steady-state planar solutions with the RANS equations. Turbulence was quantified using the two-layer realizable k-ε model [31] with Wolfstein's equation [32] in the near-wall region. The turbulence model was based on the recommendation in [33] and for performing well in reacting H2-air simulations including supersonic combustion [9] and non-premixed tank rupture situations [11].

Table 1 shows the simulated complex chemistry combustion reactions and tabulated coefficients for the Arrhenius expression

$$k = A T^N \exp \frac{-E}{R_u T} \tag{8}$$

where R_u is the universal gas constant, A is the pre-exponential factor, E is the activation energy, and N is the temperature exponent. The 2-step model proposed by Rogers and Chinitz [3] was implemented (coefficients provided in Drummond [34]) for the respective forward- and reverse reaction rates k that are related by

$$k_b = \frac{k_f}{K} \tag{9}$$

where K is the equilibrium constant.

$$K1 = 26.164 \exp -\frac{8992}{T} \tag{10}$$

$$K2 = 2.682 \times 10^{-6} T \exp \frac{69415}{T} \tag{11}$$

In general, the pre-exponential factors whose units are (mol, cm, s, K) were evaluated as functions of equivalence ratio φ

$$A1 = \left(8.917\varphi + \frac{31.433}{\varphi} - 28.95\right) 10^{47} \tag{12}$$

$$A2 = \left(2.0 + \frac{1.333}{\varphi} - 0.833\varphi\right) 10^{64} \tag{13}$$

Simulating nitrogen oxide emissions was outside the scope of this study.

Table 1. Arrehenius parameters for H2-air Rogers-Chinitz reaction mechanisms. Tabulated A values calculated using $\varphi = 1$. Coefficients from Drummond [34]

No.	Reaction	A (mol, cm, s, K)	N	E, J/kmol
f1	H2 + O2 $\rightarrow$ OH + OH	1.138e48	-10	4865
b1	H2 + O2 $\leftarrow$ OH + OH	4.349e46	-10	-7.475e8
f2	2 OH + H2 $\rightarrow$ 2 H2O	2.5e64	-13	42500
b2	2 OH + H2 $\leftarrow$ 2 H2O	9.321e69	-14	5.772e8

The five species were assumed to be ideal gases where specific heat was evaluated using thermodynamic polynomial data and dynamic viscosity and thermal conductivity were interpolated from tabulated values as a function of temperature. Material properties for the multi-component gas used the mass-weighted mixture method. Constants were assumed to be Schmidt Number=0.8, Turbulent Prandtl Number=0.9, and Turbulent Schmidt Number=0.9. Given the co-flow setup produced turbulent non-premixed flames, turbulence-chemistry interactions were modelled using the eddy dissipation concept [35]. Following the implementation by Molkov *et al.* [36] who simulated hydrogen non-premixed combustion in an enclosure, time factor=0.4082 and length factor=2.1377.

Figure 2 shows the computational domain considered in this study. Mass flow inlets with uniform flow normal to the boundary were specified for the air (0.767 N2, 0.233 O2 mass fractions) and H2 domain inlets to better inform differences in $\mathcal{T}$. The remaining air inlet specifications were $T_7 = T_0$, 5% turbulence intensity and viscosity ratio=20 whereas the H2 inlet values were $T_{H2} = 500$ K, 10% turbulence intensity and viscosity ratio=10. The plenum farfield was specified as a free stream air boundary with flow direction in x, Mach number= M_0, ambient temperature, t_{amb}, 1% turbulence intensity, and viscosity ratio=10. The downstream plenum boundary was set to a pressure outlet with pressure = 0 Pa(g).

To mimic the effects of effusion cooling through the combustor liner, a porous volume region was specified assuming the flow direction was 20 deg inwards. Inertial coefficient in the axial direction was expressed using the thin-walled perforated plate correlation available in Idelchik [37]

$$\zeta_{ax} = \frac{2\rho}{t} \frac{\left(0.707\sqrt{1-\phi} + 1 - \phi\right)^2}{\phi^2} \tag{14}$$

for t thickness where the first term is needed given the implementation in STAR-CCM+ is $\Delta ps = -\zeta |V| V$ and transverse coefficient $\zeta_{tr} = 20\zeta_{ax}$. Note that for the intended effusion holes with hole length-to-diameter ratio greater than one, an alternate correlation should be implemented to better match the

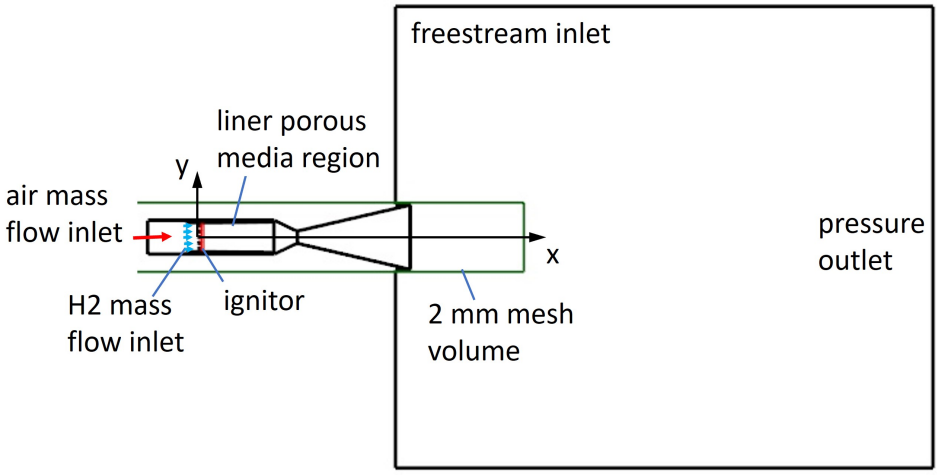

Fig 2. Computational domain.

geometry. For the purpose of this study, Eq. (14) was capable of producing W_{26} within a desirable range; however, likely has a mismatch with the quantified ϕ_{26}.

Although conduction and radiation were not explicitly modelled in this simulation, heat transfer at the walls was evaluated using the convection heat transfer coefficient

$$h_v = \begin{cases} 10 + 30\left(\frac{M_0-2}{3}\right) & \text{W/m2-K, diverging nozzle wall.} \\ 10, & \text{otherwise.} \end{cases} \tag{15}$$

with the reference temperature set to t_{amb}. The expression was interpreted from results in Cerantola, Handford and Dass [1] who proposed that the conduction coefficient should be $h_v = 10$ W/m2-K and the linear interpolation was extracted from surface-to-surface radiation exchange with the surroundings assuming 0.9 emissivity. Note that for a H2-air reaction, the flame radiative heat transfer can be neglected because of its modest optical thickness [17].

Mesh specifications were informed by preliminary CFD studies on a chemically reacting diffusion H2-air flame using the setup described in Cabra [38] and nozzles. The reacting flow CFD showed reasonable agreement in temperature magnitudes at several offset distances from the injector when the cell size=2mm; however, under-estimated the lift-off height and over-estimated the centreline flame length relative to the experimental results. It was suspected that turbulence levels instigated by the nozzle lip were enhanced whereas turbulence mixing levels in the wake were suppressed. The length predictions were also found to be sensitive to grid size. For this study, it was elected to set the average cell size in the internal components = 2 mm with 25 inflation layers and a growth rate of 1.18 where the average first cell size at Mach 5 was $y^+ = 0.5$.

The equation set was solved using the Coupled flow model where derivatives were discretized using the MUSCL 3rd-order central-differencing scheme with inviscid flux equated using AUSM+ flux-vector splitting. The discrete linear system was iteratively solved using the AMG Linear Solver using the F Cycle with 0 pre-sweeps, 3 post-sweeps, and 2 max levels. Incomplete lower-upper relaxation and bi-conjugate gradient stabilized acceleration were selected.

Solutions were initialized using grid sequencing expert initialization for each design point assuming air where the H2 injector mass fraction was initially set 100% N2. To help guide the expert initialization, pressures, temperatures, and velocities inside the duct were set to the air inlet values whereas the plenum assumed the farfield values. The initialization sequence included ramping up the injector H2 mass fraction to 100% H2 at the 10th iteration, allowing complex chemistry interactions to begin at the 50th iteration where the minimum temperature for reactions was 200 K, and a 1650 K pulsed ignitor was

triggered between iterations 50 and 200. Explicit relaxation was a constant 0.3, and Courant-Friedrichs-Lewy (CFL) number started at CFL=50 for the first 50 iterations, CFL=150 up to iteration 1000, and CFL=30 thereafter. The complex chemistry accelerator factor ramped up from 0.5 to a maximum 0.75. Solutions completed 2000 iterations in 45 min using 180 cores on AMD EPYC™ 7742 processors with a maximum frequency of 2.5 GHz and 456 GB memory per node. It was observed that temperature, Mach, mass flow, and heat balance monitors had achieved a steady value for at least the final 500 iterations.

4. Results

4.1. Baseline Study

To obtain satisfactory coverage within the flight envelope, 25 design points were simulated from $M_0 = \{3.0, 3.5, 4.0, 4.5, 5.0\}$ and $p_{dyn} = \{3, 5, 7, 9, 11\}$ psi corresponding to an altitude range 16 < alt < 30 km. Freestream Reynolds numbers per unit length increased with altitude in the range $Re_0 = 0.2$–1×10^7 m^{-1} and Prandtl number $Pr_0 = 0.73$. Angle-of-attack was set to 0 deg for all simulations. Geometric baseline values are provided in Tab. 2.

Table 2. Baseline values and ranges considered in the Geometry study. The 'I_{sp} best' is the design with the highest I_{sp} from the Geometry Study at $M_0 = 5$, $p_{dyn} = 5$ psi.

parameter	φ	BR_{FH}	χ_{FH}	θ_{FH}, deg	ΔY_{FH}, m	ΔX_{H2}, m
baseline value	0.8	0.32	1.05	15	0.075	0.15
minimum	0.7	0.22	1	10	0.05	0.05
maximum	1.1	0.42	1.1	30	0.1	0.25
I_{sp} best	0.7	0.42	1.03	15	0.05	0.1

parameter	H_{H2}, m	θ_{26}, deg	L_{26}	ϕ_{26}	H_{15}, m
baseline value	0.002	0.7	1.0	0.025	0.03
minimum	0.001	0.4	0.5	0.005	0.02
maximum	0.003	0.8	1.5	0.045	0.04
I_{sp} best	0.001	0.7	1.25	0.025	0.04

Figure 3 shows the respective properties from the baseline study at $M_0 = 5$ and $p_{dyn} = 5$ psi. The velocity field shows $M_7 = 0.14$ and $M_{H2} = 0.30$, $M \approx 0.2$ inside the combustor and acceleration through the converging-diverging nozzle from $M_8 = 1.03$ to $M_9 = 2.57$ without any flow reversal. Reynolds numbers per unit length are $Re_0 = 3.15 \times 10^6$ m^{-1}, $Re_7 = 1.05 \times 10^6$ m^{-1}, and $Re_{H2} = 3.96 \times 10^6$ m^{-1}. The wall temperature distributions show a decrease up to $x \approx 0$ m that is consistent with developing boundary layers and that the $BPR = 8$% bypassed flow is sufficient to prevent thermal mixing from raising the surface temperature above T_7. The centreline distribution shows a sharp decrease where H2 is injected, rapid increase that is associated with combustion, and maximum temperature peak at $x = 1.14$ m. The H2 contours show jets that were released from the injectors did not mix with the adjacent jets and had $\varphi > 0.1$ beyond the nozzle outlet. The chemical heat release rate contours show that the dominant energy generation regions are in the wake of the flameholders up to $x \approx 0.5$ m and at the throat. The flameholder wake region had $k = 1000$ J/kg up to $x \approx 0.2$ m and counter-rotating vortices with absolute strength $> 1e4$ s^{-1}. The converging section of the throat where OH mass fraction was above 0.005 and z-vorticity strength $> 1e4$ s^{-1} with alternating signs that coincided with the free-shear mixing regions between the hotter temperature region in the wake of the flameholders and the colder unburnt air that is visible in Fig. 4(b).

Figure 4 shows static temperature contours for the $M_0 = 3$, $p_{dyn} = 5$ psi and $M_0 = 5$, $p_{dyn} = 5$ psi cases. Common features include the temperature magnitude increase associated with combustion and poor unification of the adjacent flames that yielded visibly stratified flow through the diverging section of the nozzle. The stratification promoted additional mixing in the diverging section of the nozzle that resulted in total temperature increases from $T_8 = 1270$ K to $T_9 = 1489$ K and $T_8 = 2052$ K to $T_9 = 2493$

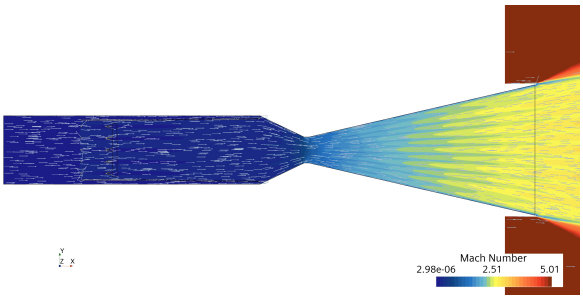

(a) Mach contours

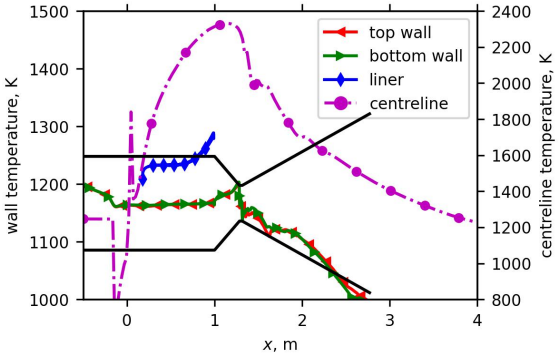

(b) Wall and centreline temperature distributions.

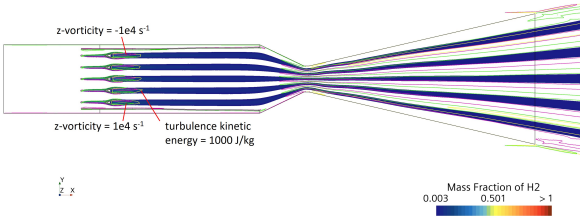

(c) Hydrogen mass fraction contours with isocontours: turbulence kinetic energy yellow=1000 J/kg, z-vorticity magenta = -1e4 s^{-1} and green=1e4 s^{-1}.

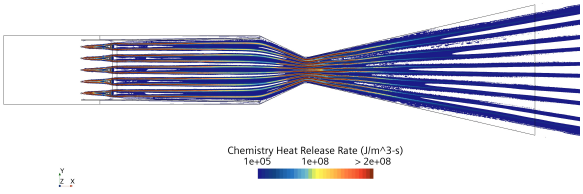

(d) Chemistry Heat Release rate contours

Fig 3. Baseline study results at Mach 5 and 5 psi.

K at the $M_0 = 3$ and $M_0 = 5$ conditions respectively. Whereas the $M_0 = 3$ condition required the auto-ignitor behind the flameholder to initialize the chemical reactions, the $M_0 = 5$ solution in Fig. 3(d) shows that heat generation began at the injector and is consistent with auto-ignition since the temperature is above the auto-ignition temperature for H2 of 833 K [39]. On a 5 psi accelerating trajectory, auto-ignition is expected to occur around $M_0 = 3.85$.

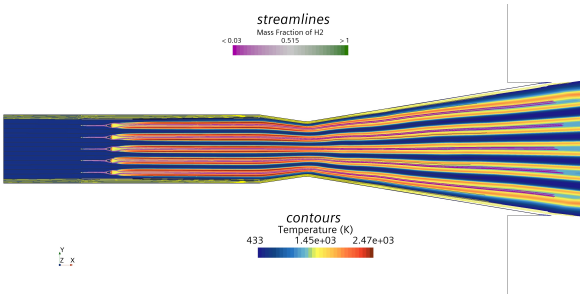

(a) Mach 3, 5 psi

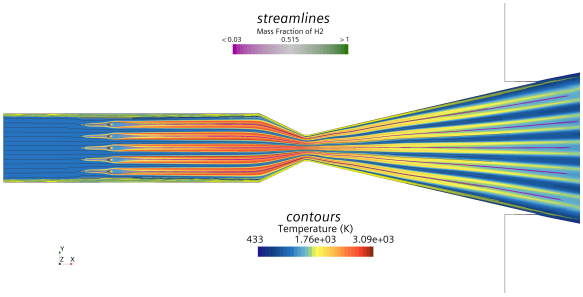

(b) Mach 5, 5 psi

Fig 4. Baseline study static temperature contours. Streamlines injected from H2 injectors coloured by H2 mass fraction.

Figure 5 shows performance metrics plotted on M_0 vs. alt maps. Values below $p_{dyn} = 3$ psi and above $p_{dyn} = 11$ psi were blanked since the parametric study did not evaluate points beyond this range. The increase in C_D with M_0 occurred due to the pressure drag increase acting on the converging section

walls where higher velocities occurred since sonic velocities were elevated due to the increased T_7 and larger downwards facing surface area of the converging section with decreased H_8. The marginal increases in C_D with alt occurred as a consequence of the lower P_7 values at lower alt that resulted in lower ρ_7 and subsequently higher U_7 and higher wall shear. The fact that I_{sp} was maximum at $M_0 = 4.5$ was due to the imposed P_7 values that resulted in minimum U_7 at $M_0 = 4.5$.

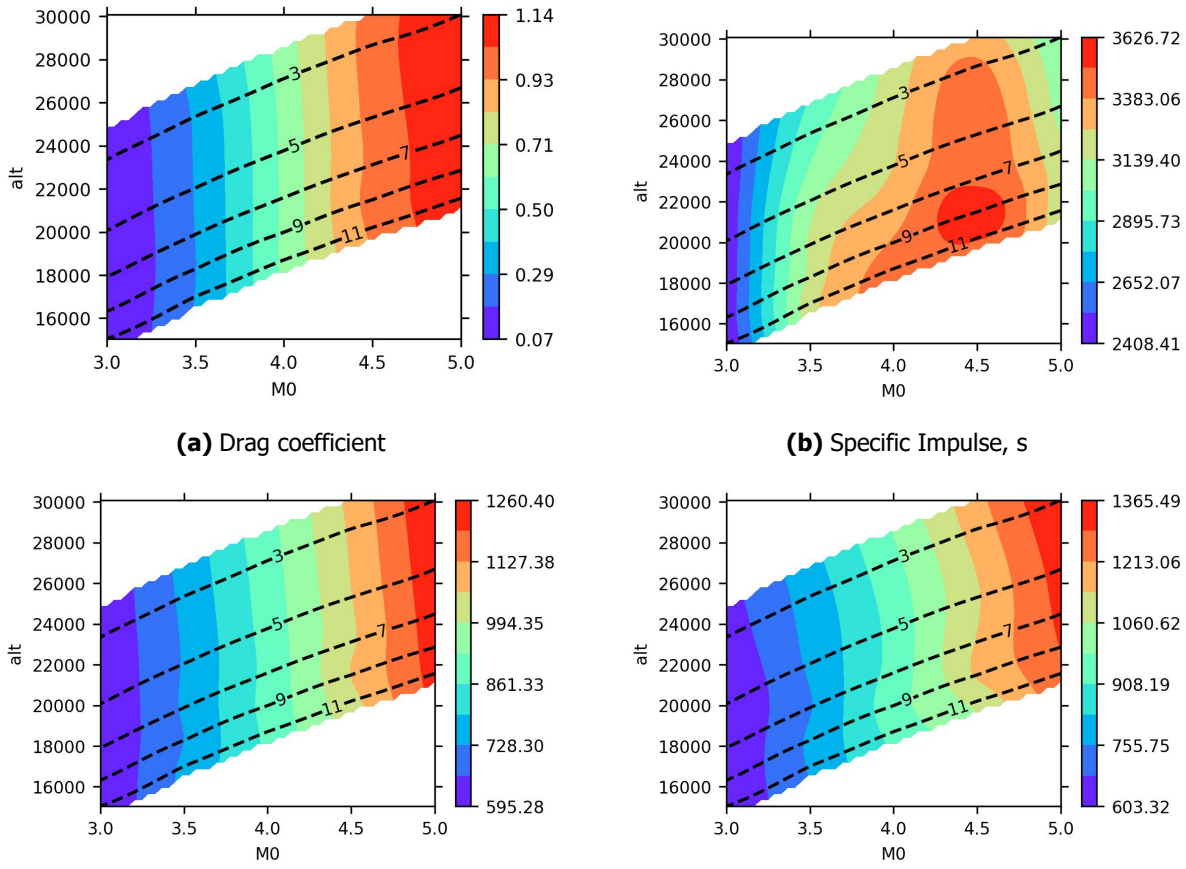

(a) Drag coefficient

(b) Specific Impulse, s

(c) Maximum wall temperature, K

(d) Maximum liner temperature, K

Fig 5. Baseline study showing performance contours on altitude vs. Flight Mach grids. Dashed lines are dynamic pressure in psi.

The maximum wall surface temperature magnitudes shown in Fig. 5(c) suggest that untreated Inconel 718 may not be adequate since 40% of its room temperature strength occurs at 1100 K [40]. Given that surface temperatures on the order of 1300 K are likely at $M_0 = 5$, materials including titanium or tungsten should be evaluated to identify a solution that maintains structural integrity with minimum weight. This is seen as a preferable option over regenerative cooling or other active thermal protection methods [41] because of the duct surface area needed for a ramjet engine. Due to the proximity to flames, it is expected that a ceramic coating will be applied to the liner where maximum surface temperature magnitudes shown in Fig. 5(d) are below thermal barrier coating (TBC) limits: Vaßen *et al.* [42] experimentally showed that their Yttria-stabilized zirconia TBC had no lifetime reduction when the surface temperature was 1770 K. Since Fry [43] reported $I_{sp} = 3900$–4200 s for H2-air between $3 < M_0 < 5$, an opportunity exists to improve the geometry to achieve higher thrust and stay below the proposed surface temperature limits of 1300 K on the walls and 1770 K on the liner.

4.2. Geometry Study

Parameter resolution for the parametric CFD study whose ranges are in Tab. 2 allowed for five possible values. Given that a full parametric study would require 5^{11} configurations per operating condition, a total sample size of 270 was instead selected where operating conditions $M_0 = 3$, $p_{dyn} = 5$ psi or $M_0 = 5$, $p_{dyn} = 5$ psi were randomly selected. Assuming a 95% confidence interval, the margin of error is 6%. This sample size is likely too small; however, a priori knowledge of the parameters influences did not exist therefore reinforcing the goal of this paper to demonstrate performance variability from coupling the combustor and nozzle components in a CFD analysis. Selection of the parameters was obtained using the Latin Hypercube function from Python's Quasi-Monte Carlo submodule [44].

Figure 6 shows the contribution of the input parameters to the responses using the LinearRegression function in the scikit-learn module [45] applied to the CFD data. The goodness of fits applied to the $M_0 = 3$ and $M_0 = 5$ datasets are respectively 0.68 and 0.72. Although there are differences in the weight magnitudes, both the $M_0 = 3$ and $M_0 = 5$ design points show strongest performance influence on L_{26}. Secondary influencers are φ towards I_{sp} and $\mathcal{T}$, H_{15} towards $ts_{max,wall}$, and ΔY_{FH} towards $ts_{max,liner}$. To better appreciate the impact of the parameters effecting responses that may influence geometric design, it is seen that $T_8 \propto (BR, \Delta Y_{FH}, L_{26})$, and strong correlations exist between Eq. (7) $L_f \propto H_{H2}$, $\forbar_{liner} \propto (L_{26}, \Delta X_{H2})$, and $C_D \propto \Delta Y_{FH}$. Although the weights influencing total pressure loss are below 20%, the top three parameters are $(P_7 - P_9)/P_7 \propto (\Delta Y_{FH}, L_{26}, \varphi)$. Interestingly, θ_{FH} and ϕ_{26} were not identified as key contributors to performance.

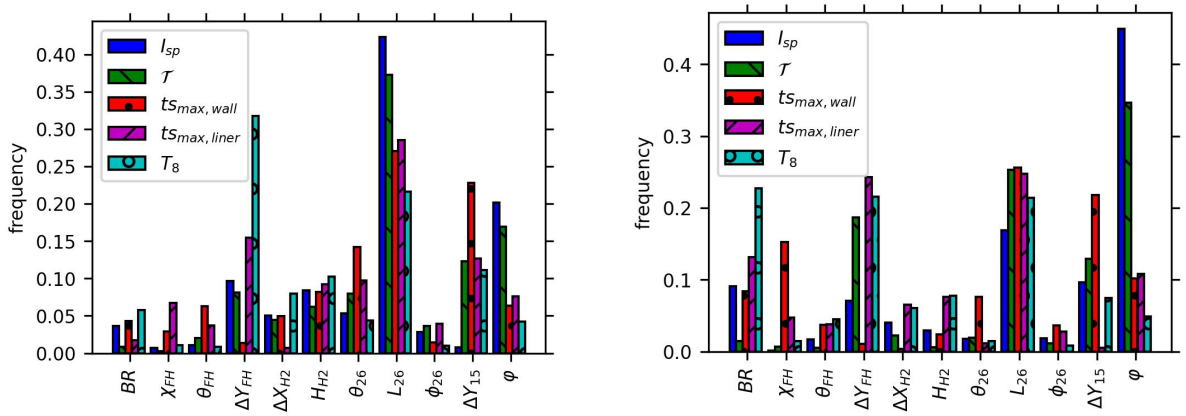

(a) Mach 3, 5 psi

(b) Mach 5, 5 psi

Fig 6. Design analysis response variability. Frequencies obtained from a linear regression function applied to the CFD sample data.

Given that the key performance metrics of interest are agnostic to the injector parameters, it can be seen from Eq. (7) on the value of minimizing H_{H2} to minimize L_f and subsequently $\forbar_{liner}$; however, given the likeliness of choked flow, increasing the number of injectors is necessary. In doing so, it is likely that through setting $\Delta X_{H2} \to 0$ and reducing L_f, $\forbar_{liner}$ can be minimized.

A surrogate model using Python's RBFInterpolator function [46] with the 'thin_plate_spline' kernal was created to interpolate performance metrics including I_{sp}, $ts_{max,wall}$, and $ts_{max,liner}$ as functions of the input parameters whose coefficients were found using the parametric CFD study. A smoothing factor = 1e-5 was applied to obtain a maximum error of the aforementioned metrics between the simulated CFD values and function values below 0.02.

Figures 7(a) and 7(b) plot I_{sp} and $\mathcal{T}$ contours estimated by the surrogate model on L_{26} vs. φ grids for the $M_0 = 5$, $p_{dyn} = 5$ psi design condition with geometry values given in Tab. 2 corresponding to the circled point. The shown magnitude ranges are appreciable and underscore the importance in removing

the interface between the combustor and nozzle to better inform design decisions. For both I_{sp} and $\mathcal{T}$, maximum performance occurs at $L_{26} = 1.5$ m; however, the trends vary with respect to φ where $\varphi = 0.7$ yields maximum I_{sp} but minimum $\mathcal{T}$. Since $I_{sp,max} = 3812$ s falls within the expected range for H2-air combustion, there is confidence that the reaction mechanism adequately predicts the theoretical heat generation.

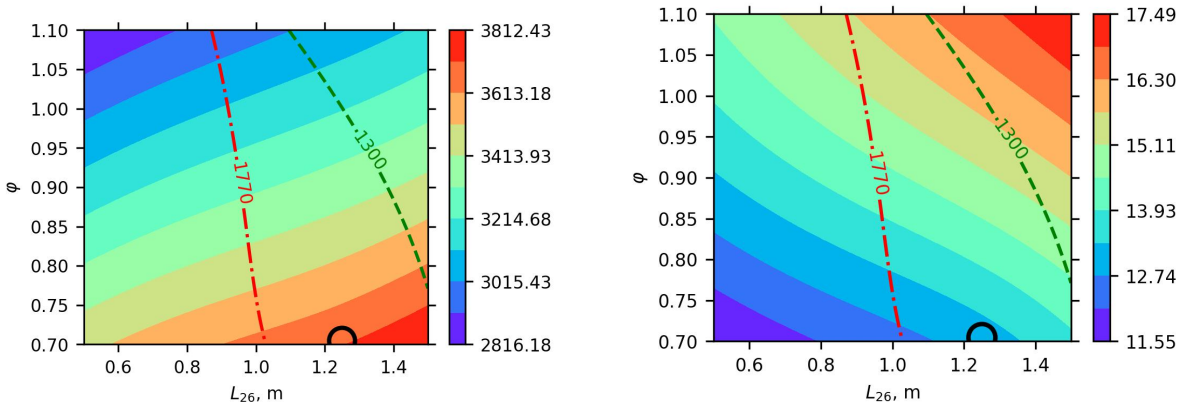

(a) Specific Impulse, s. **(b)** Net Thrust, kN.

Fig 7. Geometry study performance contours on $L26$ vs. φ grids at $M_0 = 5$ and $p_{dyn} = 5$ psi. Dashed line is $ts_{max,wall} = 1300$ K, dash-dot line is $ts_{max,liner} = 1770$ K, circled point is the 'I_{sp} best' CFD solution.

Figure 8 shows CFD temperature outcomes of the I_{sp} best case geometry at $M_0 = 5$ and $p_{dyn} = 5$ psi. The contours show the benefits of reducing ΔY_{FH} and increasing L_{26} towards increasing maximum temperature and reducing thermal stratification at the throat where the maximum centreline temperature of 2805 K occurs at $x = 1.06$ m. Despite achieving $I_{sp} = 3710$ s, this design falls short of the target $T_8 = 2700$ K temperature with $T_8 = 2285$ K and $T_9 = 2387$ K and incurs a 13% loss in thrust relative to the baseline result due to the 10% decrease in φ. Although the $BPR = 23\%$ bypassed flow maintains $ts_{max,wall} < 1245$ K, the liner hits $ts_{max,liner} = 1905$ K and therefore fails as a potential design. A possible mitigation is to increase ϕ_{26} since only $W_{26} = 0.5$ kg/s is passed through the effusion holes.

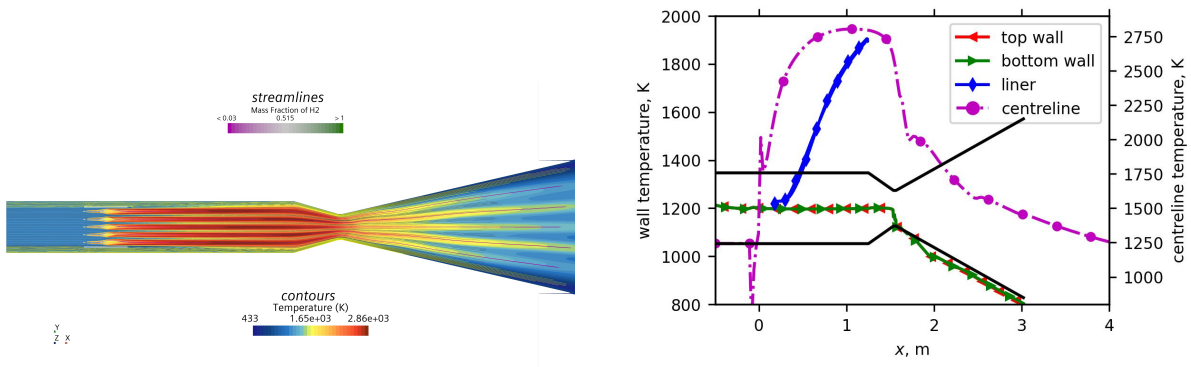

(a) Static temperature contours. Streamlines injected from H2 injectors coloured by H2 mass fraction. **(b)** Wall and centreline temperature distributions.

Fig 8. Best case temperature solution at $M_0 = 5$ and $p_{dyn} = 5$ psi.

The dashed lines in Figs. 7 correspond to surface temperatures where values to the right of the dashed line have $ts_{max,wall} > 1300$ K, and dash-dot line have $ts_{max,liner} > 1770$ K. Given material considerations, the dashed lines indicate that components will fail if $L_{26} > 1$ m. Since Eq. (7) $L_f \approx 0.7$ m at this design point, it is plausible that the 'I_{sp} best' geometry but $L_{26} \approx 1$ m is a viable solution; however, the thrust forecasted at $\varphi = 1.1$ is 10% below the indicated maximum. This is because of the amount of bypassed air where BPR linearly decreases from 0.28 to 0.20 as a function of L_{26}. Given the sparsity of this design study, continuing efforts are encouraged to obtain higher $\mathcal{T}$ where initial efforts should focus on increasing the number of injectors to reduce the length available for thermal mixing in the boundary layer.

The 'I_{sp} best' geometry evaluated at $M_0 = 3$, $p_{dyn} = 5$ psi forecasts $I_{sp,max} = 3990$ s and $\mathcal{T} = 21.6$ kN with similar contours as the $M_0 = 5$ result. At $L_{26} = 1$ m and $\varphi = 1.1$, $I_{sp} = 2630$ s and $\mathcal{T} = 17.1$ kN. In comparison to the baseline values, these 'I_{sp} best' solutions with $L_{26} = 1$ m did not appreciably change I_{sp} but $\mathcal{T}$ increased by 41% and 7% at the $M_0 = 3$ and $M_0 = 5$, $p_{dyn} = 5$ psi conditions respectively.

Given the expectation for the combustor to house the flame, at $M_0 = 3$ and $p_{dyn} = 5$ psi, $L_f \approx 0.95$ m is forecasted with the 'I_{sp} best' geometry. Since $L_{26} \approx 1$ m was identified as the maximum length for this configuration at $M_0 = 5$, this observation enforces the requirement to check the flight envelope to establish critical design points. It should also be noted that at $M_0 = 3$, BPR linearly decreases from 0.19 to 0.02 with L_{26} to indicate that there is less bypass air available to mitigate flames potentially impinging nozzle components.

5. Conclusions

Airbreathing ramjet combustor design with gaseous-hydrogen fuel must consider thrust requirements and material limitations. Through reducing assumptions from conducting a CFD study that evaluated a combustion reaction in the combustor and flow evolution through a converging-diverging nozzle, results from this study inform opportunities to improve combustor design:

- Injectors do not have a requirement to be placed at some distance upstream of the flameholders.
- Reducing the combustion chamber length is desirable to prevent thermal mixing in boundary layers from exceeding material limitations; however, longer lengths increased thrust.
- It is beneficial to increase the number of injectors so as to reduce the flame length and reduce the distance between adjacent flameholders to reduce distortion.
- Provided that it is not prohibitively expensive to source materials that can withstand 1300 K surface temperatures that are expected for Mach 5 flight, bypassing flow around a combustor liner is a film cooling option that will maintain structural integrity and achieve higher thrust.

Acknowledgements

Thanks are extended to colleagues H. DeBiasio, C. Lane, and J. McMillan for fruitful discussions about chemical kinetics, material properties, and combustor design philosophy.

References

[1] Cerantola, D. J., Handford, D., and Dass, P., "Simulating Wing Thermal Loads at Supersonic Speeds," *AIAA SCITECH 2024 Forum*, 2024, p. 2295. https://doi.org/10.2514/6.2024-2295.

[2] Varma, A. K., Chatwani, A. U., and Bracco, F. V., "Studies of premixed laminar hydrogen air flames using elementary and global kinetics models," *Combustion and flame*, Vol. 64, No. 2, 1986, pp. 233–236. https://doi.org/10.1016/0010-2180(86)90060-X.

[3] Rogers, R., and Chinitz, W., "Using a global hydrogen-air combustion model in turbulent reacting flow calculations," *AIAA Journal*, Vol. 21, No. 4, 1983, pp. 586–592. https://doi.org/10.2514/3.8117.

[4] Clutter, J., Mikolaitis, D., and Shyy, W., "Effect of reaction mechanism in shock-induced combustion simulations," *36th AIAA Aerospace Sciences Meeting and Exhibit*, 1998, p. 274. https://doi.org/10.2514/6.1998-274.

[5] Vajda, S., Rabitz, H., and Yetter, R., "Effects of thermal coupling and diffusion on the mechanism of H2 oxidation in steady premixed laminar flames," *Combustion and flame*, Vol. 82, No. 3-4, 1990, pp. 270–297. https://doi.org/10.1016/0010-2180(90)90003-A.

[6] Hsu, K., and Jemcov, A., "Numerical investigations of detonation in premixed hydrogen-air mixture-Assessment of simplified chemical mechanisms," *AIAA Fluids 2000 conference and exhibit*, 2000, p. 2478. https://doi.org/10.2514/6.2000-2478.

[7] Tabet, F., Sarh, B., and Gökalp, I., "Turbulent non-premixed hydrogen-air flame structure in the pressure range of 1–10 atm," *international journal of hydrogen energy*, Vol. 36, No. 24, 2011, pp. 15838–15850. https://doi.org/10.1016/j.ijhydene.2011.08.064.

[8] Alliche, M., and Chikh, S., "Study of non-premixed turbulent flame of hydrogen/air downstream Co-Current injector," *International Journal of Hydrogen Energy*, Vol. 43, No. 6, 2018, pp. 3577–3585. https://doi.org/10.1016/j.ijhydene.2017.06.081.

[9] Aravind, S., and Kumar, R., "Supersonic combustion of hydrogen using an improved strut injection scheme," *International Journal of Hydrogen Energy*, Vol. 44, No. 12, 2019, pp. 6257–6270. https://doi.org/10.1016/j.ijhydene.2019.01.064.

[10] Miao, J., Fan, Y., Wu, W., and Zhao, S., "Influence of air-entraining intensity on the afterburner ignition, flameholding and combustion characteristics," *Aerospace Science and Technology*, Vol. 106, 2020, p. 106063. https://doi.org/10.1016/j.ast.2020.106063.

[11] Kazemi, M., Brennan, S., and Molkov, V., "Numerical simulations of the critical diameter and flame stability for hydrogen flames," *International Journal of Hydrogen Energy*, Vol. 59, 2024, pp. 591–603. https://doi.org/10.1016/j.ijhydene.2024.02.039.

[12] Odeh, A., and Paul, M. C., "Effects of hydrogen enrichment on the heat generation and emission of natural gas turbulent premixed flame," *International Journal of Hydrogen Energy*, Vol. 49, 2024, pp. 1176–1191. https://doi.org/10.1016/j.ijhydene.2023.10.140.

[13] Fureby, C., Fedina, E., and Tegnér, J., "A computational study of supersonic combustion behind a wedge-shaped flameholder," *Shock waves*, Vol. 24, 2014, pp. 41–50. https://doi.org/10.1007/s00193-013-0459-2.

[14] Iavarone, S., Gkantonas, S., and Mastorakos, E., "Stochastic low-order modelling of hydrogen autoignition in a turbulent non-premixed flow," *Proceedings of the Combustion Institute*, Vol. 39, No. 4, 2023, pp. 5199–5208. https://doi.org/10.1016/j.proci.2022.07.129.

[15] Waluyo, R., and Aziz, M., "Advanced numerical simulation of hydrogen/air turbulent non-premixed flame on model burner," *Thermal Science and Engineering Progress*, 2024, p. 102467. https://doi.org/10.1016/j.tsep.2024.102467.

[16] Klein, M., Herbert, A., Kosaka, H., Böhm, B., Dreizler, A., Chakraborty, N., Papapostolou, V., Im, H. G., and Hasslberger, J., "Evaluation of flame area based on detailed chemistry DNS of premixed turbulent hydrogen-air flames in different regimes of combustion," *Flow, Turbulence and Combustion*, Vol. 104, 2020, pp. 403–419. https://doi.org/10.1007/s10494-019-00068-2.

[17] Gruber, A., Bothien, M. R., Ciani, A., Aditya, K., Chen, J. H., and Williams, F. A., "Direct Numerical Simulation of hydrogen combustion at auto-ignitive conditions: Ignition, stability and turbulent reaction-front velocity," *Combustion and Flame*, Vol. 229, 2021, p. 111385. https://doi.org/10.1016/j.combustflame.2021.02.031.

[18] Li, L., Yuan, Z., Xiang, Y., and Fan, A., "Numerical investigation on mixing performance and diffusion combustion characteristics of H2 and air in planar micro-combustor," *International Journal of Hydrogen Energy*, Vol. 43, No. 27, 2018, pp. 12491–12498. https://doi.org/10.1016/j.ijhydene.2018.04.194.

[19] Mbagwu, C. C., Driscoll, J. F., Dalle, D. J., and Torrez, S. M., "Combustion efficiencies and flameout limits computed for a hypersonic vehicle during ascent," *Journal of Propulsion and Power*, Vol. 34, No. 3, 2018, pp. 624–635. https://doi.org/10.2514/1.B36479.

[20] Li, H., Li, M., Chu, G., and Xiao, H., "Experimental investigation and model analysis of non-premixed hydrogen jet flames," *International Journal of Hydrogen Energy*, 2024. https://doi.org/10.1016/j.ijhydene.2024.01.143.

[21] Zhang, P., Xu, J., Quan, Z., and Mo, J., "Effects of nonuniform Mach-number entrance on scramjet nozzle flowfield and performance," *Acta Astronautica*, Vol. 129, 2016, pp. 201–210. https://doi.org/10.1016/j.actaastro.2016.09.021.

[22] Jia, X., Shan, Y., Xu, X., Zhang, J., and Tan, X., "Effects of Bypass Flow Distribution on Cold Flow Characteristics of Integrated Afterburner," *Energies*, Vol. 14, No. 18, 2021, p. 5842. https://doi.org/10.3390/en14185842.

[23] Jansen, E. T., and Thorman, H. C., "Altitude Performance Characteristics of Tail-pipe Burner with Variable-area Exhaust Nozzle," Tech. rep., National Advisory Committe for Aeronautics, Cleveland, Ohio (USA)., 1950. URL https://ntrs.nasa.gov/citations/19930086180.

[24] Groesbeck, D. E., Prince, W., and Ciepluch, C., "Evaluation of hydrogen fuel in a full-scale afterburner," Tech. rep., National Aeronautics and Space Administration, Cleveland, Ohio (USA)., 1957. URL https://ntrs.nasa.gov/citations/19650003108.

[25] Mattingly, J. D., Heiser, W. H., and Pratt, D. T., *Aircraft engine design*, 2nd ed., AIAA, 2002.

[26] Umyshev, D. R., Dostiyarov, A. M., Tumanov, M. Y., and Wang, Q., "Experimental investigation of v-gutter flameholders," *Thermal science*, Vol. 21, No. 2, 2017, pp. 1011–1019. https://doi.org/10.2298/TSCI151209072U.

[27] Cerantola, D. J., Gagnon, J., Handford, D., and Dass, P., "Design Methodology for Selecting a Single Expansion Ramp Nozzle Geometry that can Complete a Mission between Machs 3 and 7," *25th AIAA International Space Planes and Hypersonic Systems and Technologies Conference*, 2023, p. 3052. https://doi.org/10.2514/6.2023-3052.

[28] Turns, S., *An Introduction to Combustion: Concepts and Applications*, 2nd ed., McGraw-Hill Companies New York, NY, USA, 1996.

[29] Delichatsios, M., "Transition from momentum to buoyancy-controlled turbulent jet diffusion flames and flame height relationships," *Combustion and Flame*, Vol. 92, No. 4, 1993, pp. 349–364. https://doi.org/10.1016/0010-2180(93)90148-V.

[30] Siemens Digital Industries Software, "Simcenter STAR-CCM+ User Guide v. 2310," , 2024. URL https://www.plm.automation.siemens.com/global/en/products/simcenter/STAR-CCM.html.

[31] Shih, T.-H., Liou, W. W., Shabbir, A., Yang, Z., and Zhu, J., "A New k-ϵ Eddy Viscosity Model for High Reynolds Number Turbulent Flows," *Computers and Fluids*, Vol. 24, No. 3, 1995, pp. 227–238. https://doi.org/10.1016/0045-7930(94)00032-T.

[32] Wolfshtein, M., "The velocity and temperature distribution in one-dimensional flow with turbulence augmentation and pressure gradient," *International Journal of Heat and Mass Transfer*, Vol. 12, No. 3, 1969, pp. 301–318. https://doi.org/10.1016/0017-9310(69)90012-X.

[33] Siemens Digital Industries Software, "Simcenter STAR-CCM+: Best Practices for RANS Combustion," , 2019. URL https://support.sw.siemens.com/knowledge-base/KB000040311_EN_US.

[34] Drummond, J. P., *A two-dimensional numerical simulation of a supersonic, chemically reacting mixing layer*, Vol. 4055, National Aeronautics and Space Administration, Scientific and Technical Information Division, 1988. URL https://ntrs.nasa.gov/api/citations/19890003171/downloads/19890003171.pdf.

[35] Magnussen, B., "On the structure of turbulence and a generalized eddy dissipation concept for chemical reaction in turbulent flow," *19th aerospace sciences meeting*, 1981, p. 42. https://doi.org/10.2514/6.1981-42.

[36] Molkov, V., Shentsov, V., Brennan, S., and Makarov, D., "Hydrogen non-premixed combustion in enclosure with one vent and sustained release: Numerical experiments," *International journal of hydrogen energy*, Vol. 39, No. 20, 2014, pp. 10788–10801. https://doi.org/10.1016/j.ijhydene.2014.05.007.

[37] Idelchik, I., "Handbook of hydraulic resistance, 4th revised and augmented edition," *Begel House Inc., Connecticut*, 2008.

[38] Cabra, R., *Turbulent jet flames into a vitiated coflow*, University of California, Berkeley, 2003. URL https://ntrs.nasa.gov/api/citations/20040042477/downloads/20040042477.pdf.

[39] IPCS INCHEM, "Hydrogen (ICSC)," , 2021. URL https://inchem.org/documents/icsc/icsc/eics0001.htm.

[40] United States Department of Defense, "Department of Defense Handbook: Metallic materials and elements for aerospace vehicle structures," 2003.

[41] Zhang, S., Li, X., Zuo, J., Qin, J., Cheng, K., Feng, Y., and Bao, W., "Research progress on active thermal protection for hypersonic vehicles," *Progress in Aerospace Sciences*, Vol. 119, 2020, p. 100646. https://doi.org/10.1016/j.paerosci.2020.100646.

[42] Vaßen, R., Mack, D. E., Tandler, M., Sohn, Y. J., Sebold, D., and Guillon, O., "Unique performance of thermal barrier coatings made of yttria-stabilized zirconia at extreme temperatures (> 1500° C)," *Journal of the American Ceramic Society*, Vol. 104, No. 1, 2021, pp. 463–471. https://doi.org/10.1111/jace.17452.

[43] Fry, R. S., "A century of ramjet propulsion technology evolution," *Journal of propulsion and power*, Vol. 20, No. 1, 2004, pp. 27–58. https://doi.org/10.2514/1.9178.

[44] The SciPy community, *Quasi-Monte Carlo submodule, version 1.9.3*, 2022. URL https://docs.scipy.org/doc/scipy/reference/stats.qmc.html, accessed December 29, 2022.

[45] Pedregosa, F., Varoquaux, G., Gramfort, A., Michel, V., Thirion, B., Grisel, O., Blondel, M., Prettenhofer, P., Weiss, R., Dubourg, V., Vanderplas, J., Passos, A., Cournapeau, D., Brucher, M., Perrot, M., and Duchesnay, E., "Scikit-learn: Machine Learning in Python," *Journal of Machine Learning Research*, Vol. 12, 2011, pp. 2825–2830. URL https://inria.hal.science/hal-00650905.

[46] The SciPy community, *RBFInterpolator, version 1.10.1*, 2023. URL https://docs.scipy.org/doc/scipy/reference/generated/scipy.interpolate.RBFInterpolator.html, accessed March 8, 2023.